

## CHARACTERIZATION OF MOLECULAR OUTFLOWS IN THE SUBSTELLAR DOMAIN

NGOC PHAN-BAO<sup>1,2</sup>, CHIN-FEI LEE<sup>2</sup>, PAUL T.P. HO<sup>2,3</sup>, CUONG DANG-DUC<sup>1,4</sup>, DI LI<sup>5</sup>*Draft version August 21, 2014*

## ABSTRACT

We report here our latest search for molecular outflows from young brown dwarfs and very low-mass stars in nearby star-forming regions. We have observed three sources in Taurus with the Submillimeter Array and the Combined Array for Research in Millimeter-wave Astronomy at 230 GHz frequency to search for CO  $J = 2 \rightarrow 1$  outflows. We obtain a tentative detection of a redshifted and extended gas lobe at about 10 arcsec from the source GM Tau, a young brown dwarf in Taurus with an estimated mass of 73  $M_J$ , which is right below the hydrogen-burning limit. No blueshifted emission around the brown dwarf position is detected. The redshifted gas lobe that is elongated in the northeast direction suggests a possible bipolar outflow from the source with a position angle of about  $36^\circ$ . Assuming that the redshifted emission is outflow emission from GM Tau, we then estimate a molecular outflow mass in the range from  $1.9 \times 10^{-6} M_\odot$  to  $2.9 \times 10^{-5} M_\odot$  and an outflow mass-loss rate from  $2.7 \times 10^{-9} M_\odot \text{yr}^{-1}$  to  $4.1 \times 10^{-8} M_\odot \text{yr}^{-1}$ . These values are comparable to those we have observed in the young brown dwarf ISO-Oph 102 of 60  $M_J$  in  $\rho$  Ophiuchi and the very low-mass star MHO 5 of 90  $M_J$  in Taurus. Our results suggest that the outflow process in very low-mass objects is episodic with duration of a few thousand years and the outflow rate of active episodes does not significantly change for different stages of the formation process of very low-mass objects. This may provide us with important implications that clarify the formation process of brown dwarfs.

*Subject headings:* ISM: jets and outflows — ISM: individual (GM Tau, 2MASS J04141188+2811535, 2MASS J04381486+2611399) — stars: formation — stars: low mass, brown dwarfs — technique: interferometric

## 1. INTRODUCTION

Over the last nineteen years, observations of the statistical properties such as the initial mass function, velocity dispersion, multiplicity, accretion, jets (see Luhman et al. 2007 and references therein) of brown dwarfs (BD) (13–75  $M_J$ ) and very low-mass (VLM) stars ( $0.1\text{--}0.2 M_\odot$ ) (hereafter, VLM objects) in nearby star-forming regions have shown that all these properties of VLM objects form a continuum with those of low-mass stars. These observations therefore strongly support the starlike models (see Whitworth et al. 2007 and references therein) that VLM objects form in the same manner as low-mass stars. While the starlike models predict that pre-BD cores, which are produced by turbulent fragmentation of molecular clouds (Padoan & Nordlund 2004) or gravitational fragmentation (Bonnell et al. 2008), are dense enough to be gravitationally unstable, it is still unclear how the physical processes of BD formation occur at later stages, such as at class 0, I and II.

Since bipolar molecular outflows, which are ambient gas swept up by an underlying jet/wind (see Bachiller 1996; McKee & Ostriker 2007 and references therein),

are a basic component of the star formation process, studying the molecular outflow properties will therefore help us understand the BD formation mechanism. In the last few years, we have reported the first detections of bipolar molecular outflows from the class II BD ISO-Oph 102 in  $\rho$  Ophiuchi (Phan-Bao et al. 2008), the class II VLM star MHO 5 in Taurus (Phan-Bao et al. 2011). Our estimated values of outflow mass and mass loss rate in these VLM objects are over an order of magnitude smaller than the typical values in low-mass stars. These results have implied that the outflow process in VLM objects is a scaled-down version of that in low-mass stars. Our detections have also provided strong observational constraints such as velocity, size, mass and mass-loss rate of the outflow process for the simulation of BD formation (e.g., Machida et al. 2009). Although the molecular outflow process holds important clues to BD formation, however, only four detections of molecular outflows in the substellar domain have been reported so far: two molecular outflows from class 0/I proto BD and VLM candidates (L1014-IRS: Bourke et al. 2005; L1148-IRS: Kauffmann et al. 2011), one from a class II BD (ISO-Oph 102,  $\sim 60 M_J$ : Phan-Bao et al. 2008) and one from a class II VLM star (MHO 5,  $\sim 90 M_J$ : Phan-Bao et al. 2011).

In this paper, we present our millimeter observations of three class II BDs in Taurus. Sec. 2 presents our sample, Sec. 3 reports our millimeter observations and the data reduction, Sec. 4 presents the observational results, Sec. 5 discusses the outflow process and the formation mechanism of VLM objects, Sec. 6 summarizes our results.

## 2. SAMPLE SELECTION

<sup>1</sup> Department of Physics, International University-Vietnam National University HCM, Block 6, Linh Trung Ward, Thu Duc District, Ho Chi Minh City, Vietnam; pbnngoc@hcmiu.edu.vn

<sup>2</sup> Institute of Astronomy and Astrophysics, Academia Sinica, P.O. Box 23-141, Taipei 106, Taiwan, ROC; pbnngoc@asiaa.sinica.edu.tw

<sup>3</sup> Harvard-Smithsonian Center for Astrophysics, Cambridge, MA

<sup>4</sup> Faculty of Physics and Engineering Physics, University of Science-Vietnam National University HCM, 227 Nguyen Van Cu Street, District 5, Ho Chi Minh City, Vietnam

<sup>5</sup> National Astronomical Observatories, Chinese Academy of Science, Chaoyang District Datun Rd A20, Beijing, China

Our sample consists of eight targets in  $\rho$  Ophiuchi and Taurus. All of them are class II VLM objects. The observations of five of them have been reported in Phan-Bao et al. (2008, 2011).

In this paper, we present the observations of three remaining targets in Taurus (147 parsecs, see Loinard et al. 2007): GM Tau, 2MASS J041411.88+2811535 (hereafter 2M 0414) and 2MASS J043814.86+2611399 (hereafter 2M 0438). GM Tau was identified as a pre-main-sequence star Briceño et al. (1993), in the dark cloud HCL 2 or TMC 1 (e.g., Goldsmith et al. 2008) according to its position. The source was then spectroscopically classified as an M6.5 dwarf with an estimated mass of  $\sim 73 M_J$  (White & Basri 2003). GM Tau shows an obvious P Cygni profile (see Figure 4 in White & Basri 2003) with blue-shifted absorption components superposed on the H $\alpha$  accretion emission profile, which strongly indicates a mass-loss process as seen in higher mass T Tauri stars. 2M 0414 is an M6.25 dwarf of  $75 M_J$  (Luhman 2004; Muzerolle et al. 2005), the source lies in the dark cloud LDN 1495 (e.g., Goldsmith et al. 2008) according to its position. The H $\alpha$  emission of 2M 0414 also shows a clear P Cygni profile (see Figure 4 in Muzerolle et al. 2005), implying a mass-loss process occurring in the source. 2M 0438 is an M7.25 dwarf of  $70 M_J$  (Luhman 2004; Muzerolle et al. 2005), which lies in the same dark cloud as GM Tau. This BD exhibits strong forbidden emission lines (FELs) (Luhman 2004) as seen in MHO 5 that could be associated with outflow activities. They are therefore excellent targets for our search for molecular outflows in VLM objects. One should note that no detection of any cores associated with the three sources has been reported so far.

### 3. OBSERVATIONS AND DATA REDUCTION

We observed GM Tau with the Submillimeter Array (SMA), and 2M 0414 and 2M 0438 with Combined Array for Research in Millimeter-wave Astronomy (CARMA). The observing log of the three young BDs is given in Table 1.

#### 3.1. SMA observations

The SMA<sup>6</sup> receiver band at 230 GHz (see Ho et al. 2004) was used for the observations of GM Tau on 2010 October 26. Zenith opacities at 225 GHz were typically in the range 0.1–0.16. Both 4 GHz-wide sidebands, which are separated by 8 GHz, were used. The SMA correlator was configured with a high spectral resolution of 0.2 MHz ( $\sim 0.27 \text{ km s}^{-1}$ ) per channel for  $^{12}\text{CO}$ ,  $^{13}\text{CO}$ , and  $\text{C}^{18}\text{O}$   $J = 2 \rightarrow 1$  lines. For the remainder of each sideband, we set up a lower resolution of 3.25 MHz per channel. We used quasars 3C 111 and 3C 273 for gain and pass-band calibration of GM Tau, respectively. Uranus was observed for flux calibration for the target. The uncertainty in the absolute flux calibration is  $\sim 10\%$ .

We reduced and further analyzed the data with the MIR software package and the MIRIAD package adapted for the SMA, respectively. All eight SMA antennas were operated in the compact configuration, resulting in a

synthesized beam of  $3''.05 \times 2''.82$  with a position angle of  $61^\circ$  (natural weighting). The FWHM of the primary beam is about  $50''$  at the observed frequencies. The rms sensitivity was  $\sim 1 \text{ mJy}$  for the continuum and  $\sim 0.15 \text{ Jy beam}^{-1}$  per channel for the line data (Table 1).

#### 3.2. CARMA observations

We observed the two BDs 2M 0414 and 2M 0438 with CARMA at 230 GHz in 2010 August. All six 10.4 m, and nine 6.1 m antennas were operated in the D configuration. Zenith opacities at 227 GHz were in the range 0.21–0.3 and 0.23–0.27 for 2M 0414 and 2M 0438, respectively. All eight 500 MHz-wide bands (a maximum bandwidth of 4 GHz per sideband), which may be positioned independently with the IF bandwidth, were used with different spectral resolutions for  $^{12}\text{CO}$   $J = 2 \rightarrow 1$  line. The eight bands were set up in the following modes with the 2-BIT level: 8 MHz, 31 MHz and 62 MHz with 383 channels per band; 125 MHz, 250 MHz and 500 MHz with 319, 191 and 95 channels per band, respectively. These modes give a wide range of spectral resolutions from 0.03 to  $6.8 \text{ km s}^{-1}$  at 230 GHz. We observed quasar 3C 111 for gain calibration, 3C 84 and 3C 454.3 for pass-band calibration, and Uranus and 3C 84 for flux calibration. The uncertainty in the absolute flux calibration is  $\sim 20\%$ . We reduced the data with the MIRIAD package adapted for the CARMA. The synthesized beam sizes are about  $2''.09 \times 1''.69$  and  $2''.19 \times 1''.68$  using natural weighting for 2M 0414 and 2M 0438, respectively. The FWHM of the primary beam for the  $10.4 \times 6.1 \text{ m}$  antennas is about  $36''$  at 230 GHz. The rms sensitivities of the continuum and the line data are listed in Table 1.

## 4. RESULTS

#### 4.1. 2M 0414 and 2M 0438

2M 0414 and 2M 0438 are strong accretors (see Table 3 and references therein). While the H $\alpha$  emission with an obvious P Cygni profile observed in 2M 0414 (Muzerolle et al. 2005) indicates an outflow process and the presence of FELs in 2M 0438 (Luhman 2004) suggests outflow activities, our carbon monoxide ( $\text{CO}$   $J = 2 \rightarrow 1$ ) maps from CARMA data however do not reveal any outflows from 2M 0414 and 2M 0438. The non-detection of molecular outflows in these two BDs indicates three possible scenarios as discussed in Phan-Bao et al. (2011): (1) The outflow process has already stopped; (2) There is not much gas surrounding the sources; (3) The outflow process in these BDs is too weak to be detectable at the millimeter wavelengths.

For the case of 2M 0414, the outflow process has clearly been indicated in its H $\alpha$  emission, therefore, the first scenario should be ruled out. As the source is located in the dense region of  $^{12}\text{CO}$  and  $^{13}\text{CO}$   $J = 1 \rightarrow 0$  of LDN 1495 (see Figure 4 in Goldsmith et al. 2008), the second scenario is thus unlikely in this case. Finally, the bolometric luminosity of 2M 0414 is  $0.015 L_\odot$  (Luhman 2004), about 3 times less luminous than that of GM Tau ( $0.047 L_\odot$ , Luhman 2004). If we assume that the outflow force vs. bolometric luminosity correlation of proto stars (e.g., Takahashi & Ho 2012) is applicable for young BDs, this thus indicates that the outflow force of 2M 0414 would be weaker (i.e., weaker molecular outflow emission) than that of GM Tau. As a possible outflow from

<sup>6</sup> The Submillimeter Array is a joint project between the Smithsonian Astrophysical Observatory and the Academia Sinica Institute of Astronomy and Astrophysics and is funded by the Smithsonian Institution and the Academia Sinica.

GM Tau is marginally detected (see Section 4.2), therefore, the third scenario would be a reasonable explanation for the non-detection of outflows from 2M 0414.

For the case of 2M 0438, the source is also located in the dense region (see Figure 4 in Goldsmith et al. 2008) and it is close to GM Tau (at a distance of only  $\sim 2.8''$ ), the second scenario is thus very unlikely. The FELs may be associated with outflow or accretion activities, the first scenario is thus still possible. One should note that the bolometric luminosity of 2M 0438 is very low ( $0.0018 L_{\odot}$ , Luhman 2004), therefore, the outflow force is expected to be much less powerful than that of any class II BDs with molecular outflows detected so far. So, the first and the third scenarios are both possible for 2M 0438.

One should also note that we did not detect the dust continuum emission from 2M 0414 and 2M 0438 with an upper limit of about  $1\sigma$  ( $1\sigma = 1.4$  mJy for 2M 0438 and  $1.1$  mJy for 2M 0414). Our measurements are comparable within error bars to those reported in Scholz et al. (2006),  $0.91 \pm 0.65$  mJy for 2M 0414 and  $2.29 \pm 0.75$  mJy for 2M 0438.

#### 4.2. GM Tau

GM Tau is also a strong accretor with a mass accretion rate stronger than that of 2M 0414 and 2M 0438 (Table 3). Its obvious P Cygni profile of  $H\alpha$  emission strongly indicates the outflow process occurring in the BD.

The systemic velocity of GM Tau has not been available in the literature so far. To measure the systemic velocity of the BD, we extract a  $^{13}\text{CO } J = 1 \rightarrow 0$  spectrum toward GM Tau with the reprocessed FCRAO Taurus survey data from Qian et al. (2012). The FWHM of the  $^{13}\text{CO}$  line is about  $2.2 \text{ km s}^{-1}$  (Fig. 1), which is better described by two Gaussian components with peak velocities of  $5.5 \pm 0.3 \text{ km s}^{-1}$  and  $6.5 \pm 0.3 \text{ km s}^{-1}$ , respectively. The large-scale velocity gradient of  $^{13}\text{CO}$  seems to roughly follow a Larsons law-type power-law with respect to spatial scales (see Fig. 18 in Qian et al. 2012). The FWHM of the FCRAO primary beam is about  $50''$ . Within  $50''$ , it is thus normal in Taurus to have gas components moving at  $0.5\text{--}1 \text{ km s}^{-1}$  with respect to each other. The FCRAO data therefore suggests the systemic velocity of GM Tau to be in the range from  $5.5$  to  $6.5 \text{ km s}^{-1}$ . We thus take an average value of  $6.0 \text{ km s}^{-1}$  for the systemic velocity of the BD. Figure 2 presents the integrated intensity in the  $\text{CO } J = 2 \rightarrow 1$  emission towards GM Tau. Our map reveals only a redshifted ( $\sim 6.6\text{--}7.2 \text{ km s}^{-1}$ ) CO gas lobe around the BD position. No blueshifted emission is detected. It is therefore difficult to confirm that the redshifted lobe is outflow emission from GM Tau. However, the gas lobe is elongated in the northeast direction of the BD position, with a position angle of about  $36^\circ$ . This suggests that the redshifted emission is possibly outflow emission from GM Tau. One should note that the redshifted component is marginally detected at only  $4\sigma$ . Therefore, if it really comes from an outflow of the BD, the detection of the CO outflow from GM Tau should be considered as a tentative detection. Our previous detections (Phan-Bao et al. 2008, 2011) have shown that the molecular outflow in VLM objects is bipolar as seen in low-mass stars and the intensity of the outflow emission differs significantly between the redshifted and

blueshifted components. Therefore, the non-detection of blueshifted outflow emission from GM Tau is probably due to that the emission is too weak to be detected with SMA. The redshifted emission is brighter than the blueshifted emission implies that the redshifted jet propagates into denser gas than the blueshifted jet, leading to a larger swept up mass of CO gas (i.e., stronger molecular outflow emission). Deeper observations are needed to confirm this scenario.

If the detected redshifted gas lobe is a component of outflows from GM Tau, we then follow the standard manner (Cabrit & Bertout 1990; André et al. 1990) as used in the previous papers (Phan-Bao et al. 2008, 2011) to calculate the outflow properties. The size of the redshifted CO gas lobe is about  $5''$  corresponding to  $\sim 700 \text{ AU}$  in length (see Figure 2). We assume a value of  $20 \text{ K}$  for the excitation temperature, we then derive a lower limit to the outflow mass  $M_{\text{out}} \sim 1.9 \times 10^{-6} M_{\odot}$ . The correction factors due to optical depth and missing flux for the outflow mass of GM Tau are uncertain. However, the typical values of optical depths for class II objects in Taurus are from 1 to 5 (Levreault 1988a). As GM Tau lies in the densest part of HCL 2 (see Figure 4 of Goldsmith et al. 2008), therefore, it is reasonable to assume an optical depth of five for the case of GM Tau. If a missing flux factor of three for SMA (Bourke et al. 2005) is applicable here, we then obtain an upper limit to the outflow mass of  $\sim 2.9 \times 10^{-5} M_{\odot}$ .

The maximum outflow velocity  $v_{\text{max}}$  can be computed from the observed maximum outflow velocity and the outflow inclination. The observed maximum outflow velocity is about  $1.2 \text{ km s}^{-1}$ . Based on optical, near-infrared and infrared data, Riaz et al. (2012) performed disk modelling for GM Tau with a circumstellar geometry consisting of a rotationally flattened infalling envelope, bipolar cavities, and a flared accretion disk in hydrostatic equilibrium. Their best-fitting model SED was obtained with the disk's inclination angle between  $70^\circ$  and  $80^\circ$ . We therefore use an average value of  $75^\circ$  for the outflow inclination (the angle between the outflow axis and the line of sight). From the observed maximum outflow velocity of  $1.2 \text{ km s}^{-1}$  and the outflow inclination angle  $i = 75^\circ$ , we derive the maximum outflow velocity  $v_{\text{max}} = 4.6 \text{ km s}^{-1}$ . We then use this value to compute upper limit values for the kinematic and dynamic parameters. We find the momentum  $P = 8.7 \times 10^{-6} M_{\odot} \text{ km s}^{-1}$ , the energy  $E = 2.0 \times 10^{-5} M_{\odot} \text{ km}^2 \text{ s}^{-2}$ . From the outflow size of  $\sim 700 \text{ AU}$  and the observed maximum outflow velocity of  $1.2 \text{ km s}^{-1}$ , we derive the dynamical time  $t_{\text{dyn}}$  for GM Tau of about  $700 \text{ yr}$  (with a correction for the outflow inclination). With this dynamical time value, we then find the force  $F = 1.2 \times 10^{-8} M_{\odot} \text{ km s}^{-1} \text{ yr}^{-1}$ , and the mechanical luminosity  $L = 4.7 \times 10^{-6} L_{\odot}$ , where  $L_{\odot}$  is the solar luminosity. If we apply a correction for the optical depth factor of five and the missing flux factor of three for SMA, these upper limit values will increase by a factor of fifteen. Lower limits to these parameters could be estimated by using the outflow mass in each velocity channel and the space velocity of the outflow, which is assumed to be equal to the radial velocity of that channel, as if the gas was moving along the line of sight (Cabrit & Bertout 1990). This could be done for observations with good signal-to-noise ratio. However, as

our detection levels of outflows in each velocity channel are rather low, we therefore do not estimate these lower limits.

The mass-loss rate of molecular outflows can be computed by dividing the outflow mass by the dynamical time of the outflow. However, the estimated dynamical time  $t_{\text{dyn}} \sim 700$  yr for the outflow from GM Tau is over two orders of magnitude smaller than the age of VLM objects in Taurus expected to be from a few  $10^5$  yr to a few Myrs (Muzerolle et al. 2003; White & Basri 2003). Therefore, the correction factor of about ten applying for the outflow dynamical time of young low-mass stars (Parker et al. 1991) may be not valid here. This value for VLM objects should be over a hundred (see further discussion in Sec. 5.1). Without correction applied for the outflow dynamical time and using the lower and upper values of the outflow mass, we directly derive lower and upper limits to the mass-loss rate of molecular outflows  $\dot{M}_{\text{mol}} = M_{\text{out}}/t_{\text{dyn}}$  to be  $2.7 \times 10^{-9} M_{\odot} \text{ yr}^{-1}$  and  $4.1 \times 10^{-8} M_{\odot} \text{ yr}^{-1}$ , respectively.

We now consider the possibility that the detected redshifted emission might be due to gravitationally bound motion and not outflow emission. For gravitationally bound motion, an outflow size  $l = 700$  AU with a velocity  $v = 4.6 \text{ km s}^{-1}$  would require an enclosed mass of  $\geq 8.4 M_{\odot}$  ( $M \geq v^2 l / 2G$ , see Lada 1985). If we assume that the densest cores in Taurus have been detected by Onishi et al. (2002) (see their Table 2), we then derive a possible largest mass of  $\sim 0.003 M_{\odot}$  for a core of 700 AU in diameter. In addition, we also estimate an upper limit to the mass of a core of 700 AU using the gas density around the GM Tau position, which is estimated from the FCRAO observations (Qian et al. 2012). The line intensity ratio between  $^{12}\text{CO } J = 1 \rightarrow 0$  and  $^{13}\text{CO } J = 1 \rightarrow 0$  is much smaller than the corresponding isotopic ratio, thus it is safe to assume that the  $^{12}\text{CO}$  line is optically thick. We then derive the gas excitation temperature of about 10 K based on the peak antenna temperature of  $^{12}\text{CO}$ . The  $^{13}\text{CO}$  opacity, and in turn, the gas column density can then be derived by assuming a  $[^{13}\text{CO}]/[\text{H}_2]$  abundance ratio of  $1.7 \times 10^{-6}$  (Frerking et al. 1982). The resulting  $\text{H}_2$  column density is  $6.0 \times 10^{21} \text{ cm}^{-2}$ , which is consistent with 2MASS extinction measurement on arcminute spatial scale (Qian et al. 2012). Using the measured  $\text{H}_2$  column density and the FWHM of the FCRAO primary beam, we finally obtain an upper limit of  $\sim 0.13 M_{\odot}$  to a core of 700 AU within  $25''$  from the GM Tau position. Both the estimated masses from the Onishi et al. (2002) observations and FCRAO are well below the enclosed mass of  $8.4 M_{\odot}$  required for gravitational bound motion. We therefore conclude that the detected emission is from the outflow.

One should note that we did not detect the dust continuum emission with an upper limit of 1 mJy ( $= 1\sigma$ ) measured at the GM Tau position.

## 5. MOLECULAR OUTFLOWS FROM VLM OBJECTS

### 5.1. Molecular outflow properties

So far, we have observed eight VLM objects and detected three of them having CO molecular outflows: ISO-Oph 102 in  $\rho$  Ophiuchi (Phan-Bao et al. 2008), MHO 5 (Phan-Bao et al. 2011) and GM Tau (this paper) in Taurus. The molecular outflows from these three sources

show similar molecular outflow properties: small scale of 600–1000 AU, low velocity of  $< 5 \text{ km s}^{-1}$  (with a correction of outflow inclination), tiny outflow mass of  $10^{-6}$ – $10^{-4} M_{\odot}$  and low mass-loss rate of  $10^{-9}$ – $10^{-7} M_{\odot} \text{ yr}^{-1}$ . Table 2 lists these properties for each source. Our molecular outflow mass estimates in VLM objects are smaller than the typical values 0.01–0.7  $M_{\odot}$  of class II low-mass stars (G, K spectral types; see Levreault 1988b and references therein) by over an order of magnitude.

To estimate the mass-loss rate of the stellar wind that drives the molecular outflow in the VLM objects, we can assume that the stellar wind-molecular gas interaction is momentum-conserving (e.g., Levreault 1988b; André et al. 1990). We thus equate the momentum  $P = M_{\text{out}} v_{\text{max}}$  of the molecular outflow with that supplied by the wind over the outflow’s lifetime ( $\dot{M}_{\text{wind}} t_{\text{dyn}} v_{\text{wind}}$ ). This yields the expression  $\dot{M}_{\text{wind}} = M_{\text{out}} v_{\text{max}} / (t_{\text{dyn}} v_{\text{wind}})$ , where  $v_{\text{wind}}$  is the wind velocity. For ISO-Oph 102, the wind velocity is  $\sim 107 \text{ km s}^{-1}$ , which is estimated from  $v_{\text{jet}} = 45 \text{ km s}^{-1}$  (Whelan et al. 2005) with a correction of outflow inclination of  $\sim 65^\circ$  to the line of sight (Phan-Bao et al. 2008). For the cases of MHO 5 and GM Tau, as no measurements of wind velocities have been reported so far, so we assume a wind velocity of about  $100 \text{ km s}^{-1}$  for these two objects. Using the upper and lower limit values of outflow mass (see Table 2), we derive the upper and lower limits (Table 3) to the wind mass-loss rates of the VLM objects, respectively.

There is a possibility that our values of wind mass-loss rates are underestimated if the momentum from the wind might not be transferred all to the molecular gas. This happens when there is less molecular gas surrounding the source at late stages (class II) than early stages (class 0, I). However, the wind mass-loss rates of VLM objects (e.g., ISO-Oph 102) estimated from molecular outflows (see Table 2) are comparable to those derived from optical jets using the spectro-astrometric method (see Table 6 in Whelan et al. 2009, Whelan et al. 2014). This implies that our values are not significantly underestimated. All these values of wind mass-loss rates of VLM objects are smaller than a typical value of  $\sim 10^{-7} M_{\odot} \text{ yr}^{-1}$  for class-II low-mass stars of 0.5–5.0  $M_{\odot}$  (Levreault 1988a) by over about an order of magnitude (see Figure 3). Our results have shown that the outflow process occurs in VLM objects is a scaled-down version of that in low-mass stars.

One should discuss here that the ratios of wind mass-loss rate to mass accretion rate  $\dot{M}_{\text{wind}}/\dot{M}_{\text{acc}}$  in ISO-Oph 102, MHO 5 (see Table 3) are significantly higher than that in T Tauri stars ( $\sim 0.0003$ –0.4, Hartigan et al. 1995). These high ratio values imply three possible scenarios:

(1) First, we might underestimate the accretion rates as the accretion rates measured in the VLM objects at different epochs may vary over an order of magnitude on timescales of months to years (e.g., Stelzer et al. 2007). Therefore, the rates measured at particular epochs do not reflect the long-term accretion rates that are more appropriate for comparison with the outflow rates in the two VLM objects. However, the accretion rate in MHO 5 measured at different epochs has suggested that the accretion rate is stable,  $\sim 10^{-10.8} M_{\odot} \text{ yr}^{-1}$

(Muzerolle et al. 2003; Herczeg & Hillenbrand 2008). In the case of ISO-Oph 102, the accretion rate of  $\sim 10^{-9.0} M_{\odot} \text{ yr}^{-1}$  was measured at epoch 2003.411 (Natta et al. 2004), and an increase of the accretion rate by a factor of five within a week was also observed (Natta et al. 2004). However, the accretion rate of  $10^{-9.17} M_{\odot} \text{ yr}^{-1}$  (Gatti et al. 2006) measured at epoch 2005.384 agrees with the Natta et al.'s measurement, suggesting a long-term accretion rate in ISO-Oph 012 of  $\sim 10^{-9.0} M_{\odot} \text{ yr}^{-1}$ . Therefore, this scenario is unlikely the case here.

(2) Second, we might overestimate the wind mass-loss rate. This is due to that we did not apply a correction factor for the dynamical time (see Table 3). If the estimated dynamical time is a lower limit to the real dynamical time, we then need to apply a correction factor of about 100 for the case of ISO-Oph 102 and 1000 for MHO 5 as well as GM Tau (see Section 5.2 for further discussion), instead of 10 as estimated for low-mass stars (Parker et al. 1991), for the outflow dynamical time of VLM objects. The wind mass-loss rates, hence, the ratios  $\dot{M}_{\text{wind}}/\dot{M}_{\text{acc}}$  will decrease by the same factors and they are thus comparable to those in T Tauri stars.

(3) Third, this ratio in VLM objects is really higher than that in low-mass stars. This is possibly due to a sudden drop of the mass accretion rate during the formation process of brown dwarfs as proposed by Machida et al. (2009). Further observations and theoretical works are needed to confirm these possible scenarios.

### 5.2. Episodic outflows?

The outflow dynamical times estimated for the three class-II VLM objects, ISO-Oph 102 (Phan-Bao et al. 2008), MHO 5 (Phan-Bao et al. 2011) and GM Tau (this paper) are from  $7.0 \times 10^2 \text{ yr}$  to  $2.7 \times 10^3 \text{ yr}$  (see Table 2). These values are still about two or three orders of magnitude smaller than the ages of ISO-Oph 102, GM Tau and MHO 5 expected to be from a few  $10^5 \text{ yr}$  (ISO-Oph 102, Natta et al. 2004) to a few Myr (GM Tau and MHO 5, see Muzerolle et al. 2003 and references therein).

The extreme discrepancy between the outflow dynamical time and the age of the VLM objects indicates two possibilities:

(1) The extent of outflows is not completely revealed because of the coverage and the sensitivity of our observations. For example, an outflow with velocity of  $5 \text{ km s}^{-1}$  and a dynamical time of  $10^5 \text{ yr}$  will have a length of about 0.5 pc, or  $12'$  at the distance of Taurus. This is more than an order of magnitude larger than the SMA primary beam size. Therefore, any molecular outflow emission that lies more than half a primary beam from the source would be impossible to detect. In addition, the full extent of outflows to the edge of the primary beam has not been detected (e.g., ISO-Oph 102, see Fig. 1 in Phan-Bao et al. 2008), which is possibly due to the sensitivity limit of SMA. The estimated outflow dynamical time is thus a lower limit to the true outflow duration as discussed in Parker et al. (1991) for the case of low-mass stars.

(2) The outflow process in the VLM objects is episodic, occurring in class II with duration of a few  $10^3 \text{ yr}$ . An episodic outflow will have a discrete blob morphology. In this case, other blobs of the molecular outflows from our

VLM objects that lie outside the primary beam would not be detected. The outflows detected by SMA are thus from the last active episodes. If the episodicity of these outflows is confirmed, the outflow process in VLM objects will include quiescent and active episodes. One then can expect that the accretion associated with outflow is also episodic. This is consistent with evolutionary models as proposed by Baraffe et al. (2009) that the accretion process in BDs at early stages could be episodic, including long quiescent phases of accretion interrupted by short episodes (a few  $10^3$  to  $10^4 \text{ yr}$ ) of high accretion. Their evolutionary models taking into account episodic phases of accretion successfully explain the significant luminosity spread observed in H-R diagrams of star-forming regions.

More extended and deeper observations are therefore needed to explore the morphology of the outflows from these VLM objects in order to confirm the scenarios.

### 5.3. Molecular outflows and the formation of VLM objects

The outflow masses and the mass-loss rates of the molecular outflows from ISO-Oph 102, GM Tau and MHO 5, which are class II objects, are comparable to those of L1014-IRS (Bourke et al. 2005), a proto BD candidate at a younger age (class 0/I) that has an outflow with a mass and mass-loss rate of  $\sim 10^{-5} M_{\odot}$  and  $\sim 10^{-9} M_{\odot} \text{ yr}^{-1}$ , respectively. In the case of the class I proto BD candidate L1148-IRS (Kauffmann et al. 2011), the outflow mass ( $\sim 10^{-3} M_{\odot}$ ) and the mass-loss rate ( $\sim 10^{-7} M_{\odot} \text{ yr}^{-1}$ ) are slightly larger than that from our VLM objects but still comparable to the range of our lower and upper limits (see Table 2). This similarity implies that the mass-loss rate, hence the associated wind mass-loss and accretion rates in VLM objects do not significantly change in different formation stages (from class 0/I to class II).

As discussed in Section 5.1, the ratio of wind mass-loss rate to accretion rate  $\dot{M}_{\text{wind}}/\dot{M}_{\text{acc}}$  in VLM objects is possibly higher than that in low-mass stars (Table 3). If the wind mass-loss rate does not significantly change for different classes of VLM object formation,  $10^{-11}$ – $10^{-8} M_{\odot} \text{ yr}^{-1}$  (see Table 3), then, one may expect that this ratio also holds in earlier classes, such as classes 0, I. This suggests that the accretion rate in VLM objects expected to be also in the range  $10^{-11}$ – $10^{-9} M_{\odot} \text{ yr}^{-1}$  at earlier stages. The starlike models for BD formation predict that VLM cores produced by fragmentation (Padoan & Nordlund 2004; Bonnell et al. 2008) are dense enough to be gravitationally unstable. The detection of such a VLM core (André et al. 2012) supports these models. Our observations suggest that these VLM cores may undergo some active episodes of outflow and associated accretion with duration of a few  $10^3 \text{ yr}$ . The accretion rates, however, are very low, in the range  $10^{-11}$ – $10^{-9} M_{\odot} \text{ yr}^{-1}$  or lower, and they are comparable or smaller than the mass-loss rate. This may therefore prevent the VLM cores to accrete enough material to become a star.

## 6. SUMMARY

Here, we report our latest search for molecular outflows from VLM objects. So far, we have detected molecular

outflows from two BDs (one in  $\rho$  Ophiuchi and one in Taurus) and one VLM star in Taurus. Our results suggest that: (1) the bipolar molecular outflow process in VLM objects is a scaled-down version of that in low-mass stars; (2) the outflow mass-loss and the associated mass accretion processes in VLM objects are possibly episodic with duration of a few thousand years; (3) the outflow mass-loss rate and the mass accretion rate during active episodes are very low and they do not significantly change for different stages of the formation process of VLM objects; (4) A very low mass accretion rate, possibly together with a high ratio of outflow mass-loss rate to mass accretion rate, may prevent a VLM core to accrete enough gas to become a star; and thus the core will end up a BD.

This research is funded by Vietnam National Foundation for Science and Technology Development (NAFOS-TED) under grant number 103.08-2013.21. D.L. acknowledges the support from National Basic Research Program of China (973 program) No. 2012CB821800 and NSFC No. 11373038. We thank the referee for valuable comments. Support for CARMA construction was derived from the Gordon and Betty Moore Foundation, the Kenneth T. and Eileen L. Norris Foundation, the James S. McDonnell Foundation, the Associates of the California Institute of Technology, the University of Chicago, the states of California, Illinois, and Maryland, and the National Science Foundation. Ongoing CARMA development and operations are supported by the National Science Foundation under a cooperative agreement, and by the CARMA partner universities.

## REFERENCES

- André, P., Martín-Pintado, J., Despois, D., & Montmerle, T. 1990, *A&A*, 236, 180
- André, P., Ward-Thompson, D., & Greaves, J. 2012, *Science*, 337, 69
- Bachiller, R. 1996, *ARA&A*, 34, 111
- Baraffe, I., Chabrier, G., & Gallardo, J. 2009, *ApJ*, 702, L27
- Bonnell, I. A., Clark, P., & Bate, M. R. 2008, *MNRAS*, 389, 1556
- Bourke, T. L., Crapsi, A., Myers, P. C., Evans, Neal J., II, Wilner, D. J., Huard, T. L., Jørgensen, J. K., & Young, C. H. 2005, *ApJ*, 633, L129
- Briceño, C., Calvet, N., Gomez, M., Hartmann, L. W., Kenyon, S. J., & Whitney, B. A. 1993, *PASP*, 105, 686
- Cabrit, S., Goldsmith, P. F., & Snell, R. L. 1988, *ApJ*, 334, 196
- Cabrit, S., & Bertout, C. 1990, *ApJ*, 348, 530
- Freking, M. A., Langer, W. D., & Wilson, R. W. 1982, *ApJ*, 262, 590
- Gatti, T., Testi, L., Natta, A., Randich, S., & Muzerolle, J. 2006, *Å*, 460, 547
- Goldsmith, P. F., Heyer, M., Narayanan, G., Snell, R., Li, D., & Brunt, C. 2008, *ApJ*, 680, 428
- Hartigan, P., Edwards, S., & Ghandour, L. 1995, *ApJ*, 452, 736
- Herczeg, G. J., & Hillenbrand, L. A. 2008, *ApJ*, 681, 594
- Ho, P. T. P., Moran, J. M., & Lo, K. Y. 2004, *ApJ*, 616, L1
- Kauffmann, J., Bertoldi, F., Bourke, T. L., Myers, P. C., Lee, C. W., & Huard, T. L. 2011, *MNRAS*, 416, 2341
- Lada, C. J. 1985, *ARA&A*, 23, 267
- Levreault, R. M. 1988a, *ApJS*, 67, 283
- Levreault, R. M. 1988b, *ApJ*, 330, 897
- Loinard, L., Torres, R. M., Mioduszewski, A. J., Rodríguez, L. F., González-Lópezlira, R. A., Lachaume, R., Vázquez, V., & González, E. 2007, *ApJ*, 671, 546
- Luhman, K. L. 2004, *ApJ*, 617, 1216
- Luhman, K. L., Joergens, V., Lada, C., Muzerolle, J., Pascucci, I., & White, R. 2007, in *Protostars and Planets V*, ed. B. Reipurth, D. Jewitt, & K. Keil (Tucson: Univ. Arizona Press), 443
- Machida, M. N., Inutsuka, S., & Matsumoto, T. 2009, *ApJ*, 699, L157
- McKee, C. F., & Ostriker, E. C. 2007, *ARA&A*, 45, 565
- Muzerolle, J., Hillenbrand, L., Calvet, N., Briceño, C., & Hartmann, L. 2003, *ApJ*, 592, 266
- Muzerolle, J., Luhman, K. L., Briceño, C., Hartmann, L., & Calvet, N. 2005, *ApJ*, 625, 906
- Narayanan, G., Heyer, M. H., Brunt, C., Goldsmith, P. F., Snell, R., & Li, D. 2008, *ApJS*, 177, 341
- Natta, A., Testi, L., Muzerolle, J., Randich, S., Comerón, F., & Persi, P. 2004, *A&A*, 424, 603
- Onishi, T., Mizuno, A., Kawamura, A., Ogawa, H., & Fukui, Y. 2002, *ApJ*, 575, 950
- Padoan, P., & Nordlund, Å. 2004, *ApJ*, 617, 559
- Parker, N. D., Padman, R., & Scott, P. F. 1991, *MNRAS*, 252, 442
- Phan-Bao, N., et al. 2008, *ApJ*, 689, L141
- Phan-Bao, N., Lee, C.-F., Ho, P. T. P., & Tang, Y.-W. 2011, *ApJ*, 735, 14
- Qian, L., Li, D., & Goldsmith, P. F. 2012, *ApJ*, 760, 147
- Riaz, B., Honda, M., Campins, H., Micela, G., Guarcello, M. G., Gledhill, T., Hough, J., & Martín, E. L. 2012, *MNRAS*, 420, 2603
- Scholz, A., Jayawardhana, R., & Wood, K. 2006, *ApJ*, 645, 1498
- Stelzer, B., Scholz, A., & Jayawardhana, R. 2007, *ApJ*, 671, 842
- Takahashi, S., & Ho, P. T. P. 2012, *ApJ*, 745, L10
- Whelan, E. T., Ray, T. P., Bacciotti, F., Natta, A., Testi, L., Randich, S. 2005, *Nature*, 435, 652
- Whelan, E. T., Ray, T. P., Randich, S., Bacciotti, F., Jayawardhana, R., Testi, L., Natta, A., & Mohanty, S. 2007, *ApJ*, 659, L45
- Whelan, E. T., Ray, T. P., Podio, L., Bacciotti, F., & Randich, S. 2009, *ApJ*, 706, 1054
- Whelan, E. T., et al. 2014, *A&A*, 565, A80
- White, R. J., & Basri, G., 2003, *ApJ*, 582, 1109
- Whitworth, A., Bate, M. R., Nordlund, Å., Reipurth, B., & Zinnecker, H. 2007, in *Protostars and Planets V*, ed. B. Reipurth, D. Jewitt, & K. Keil (Tucson: Univ. Arizona Press), 459

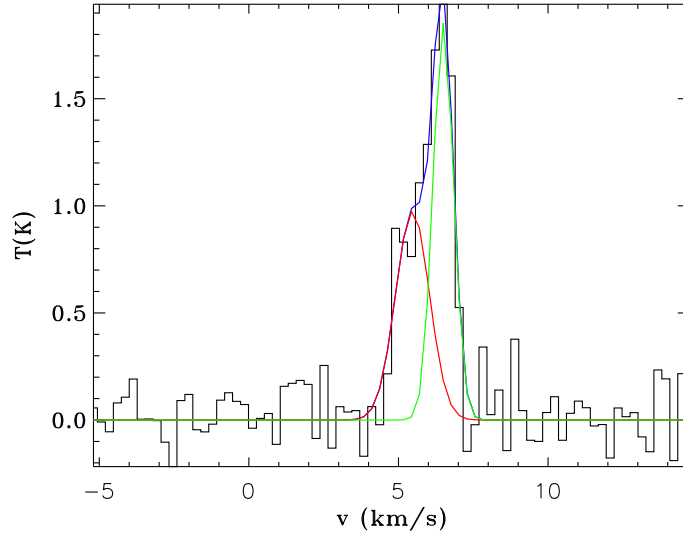


FIG. 1.— The  $^{13}\text{CO } J = 1 \rightarrow 0$  spectrum toward GM Tau overlaid with two Gaussian components,  $5.5 \text{ km s}^{-1}$  (red line) and  $6.5 \text{ km s}^{-1}$  (green line). The data were taken from Qian et al. (2012), which was part of the FCRAO survey by Goldsmith et al. (2008) and reprocessed with a better deconvolution. The FWHM of the FCRAO primary beam is about  $50''$ .

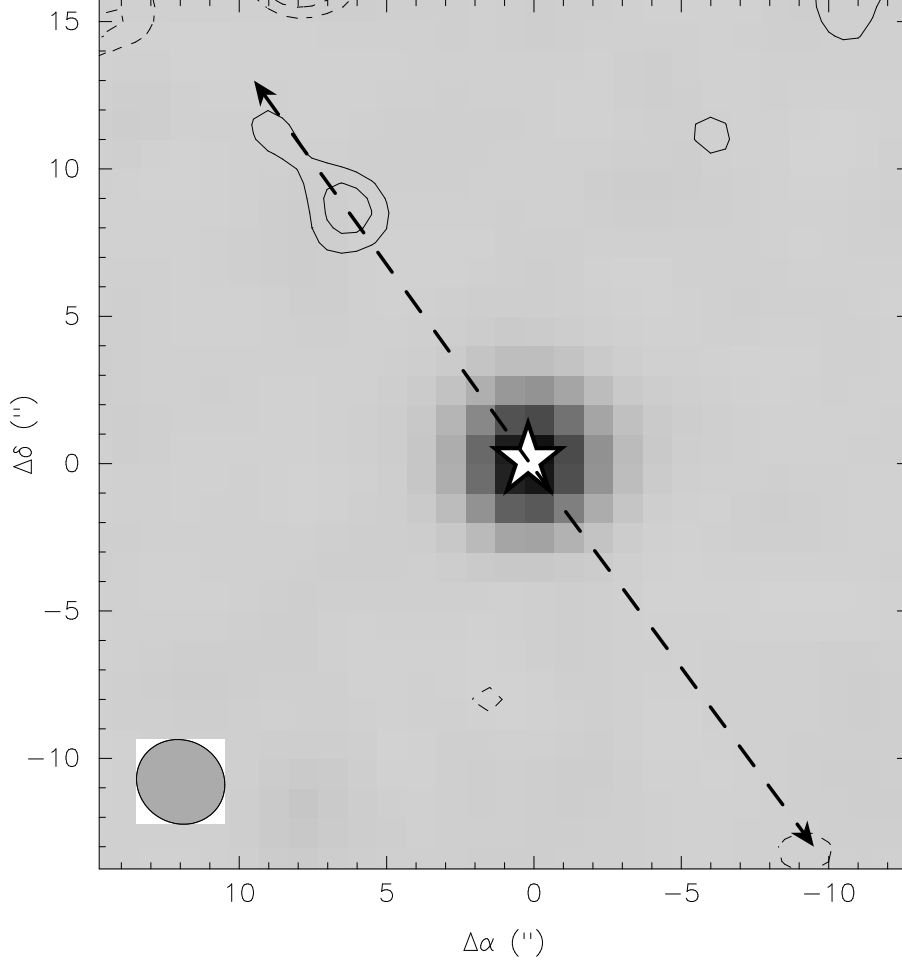


FIG. 2.— Overlay of the J-band ( $1.25\ \mu\text{m}$ ) near-infrared Two Micron All Sky Survey image and the integrated intensity in the CO  $J = 2 \rightarrow 1$  line emission from  $6.6$  to  $7.2\ \text{km s}^{-1}$  line-of-sight velocities towards GM Tau. The contours are  $-4, -3, 3, 4, \dots$  times the rms of  $0.05\ \text{Jy beam}^{-1}\ \text{km s}^{-1}$ . The source is visible in the near-infrared image. The position angle of the outflow is about  $36^\circ$ . The expected outflow direction is indicated by the arrows. The star symbol represents the BD position. The synthesized beam is shown in the bottom left corner.



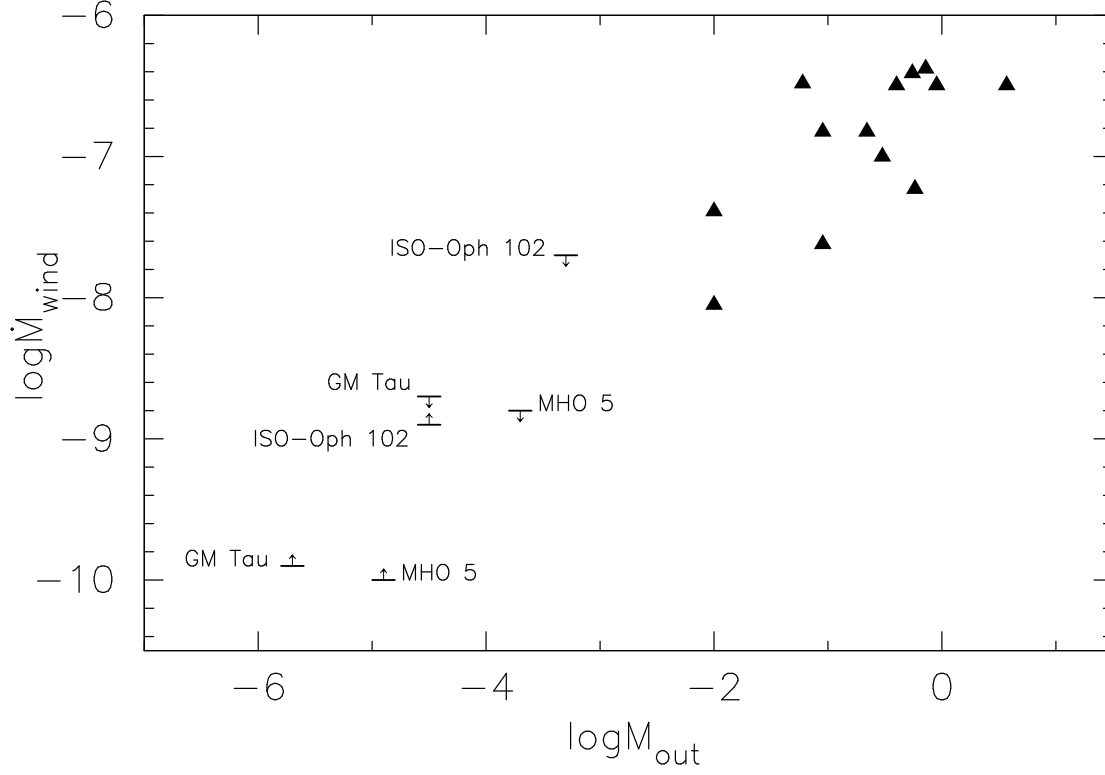


FIG. 3.— Comparison between the molecular outflow mass and the wind mass-loss rate of VLM objects and low-mass stars. The arrows up and down indicate the lower and upper limits, respectively. Solid triangles represent class II low-mass stars with masses of  $0.5\text{--}5.0 M_{\odot}$  (Levreault 1988a).

TABLE 1  
OBSERVING LOGS FOR THE THREE YOUNG BDs IN TAURUS

Target	Array	Configuration	Beam size ( $" \times "$ )	continuum rms (mJy/beam)	line rms (Jy/beam)	velocity resolution (km s $^{-1}$ )
2M 0438	CARMA	D	2.19 $\times$ 1.68	1.4	0.20	0.11
GM Tau	SMA	Compact	3.05 $\times$ 2.82	1.0	0.15	0.27
2M 0414	CARMA	D	2.09 $\times$ 1.69	1.1	0.13	0.11

NOTE. — For 2M 0438 and 2M 0414, line rms and velocity resolution are computed for bandwidth 31 MHz.

TABLE 2  
MOLECULAR OUTFLOW PROPERTIES OF CLASS II VLM OBJECTS IN  $\rho$  OPHIUCHI AND TAURUS

Target	Array	Mass ( $M_J$ )	Region	size (length) (AU)	$v_{\max}$ (km s $^{-1}$ )	$\log M_{\text{out}}^{\text{a}}$ ( $M_{\odot}$ )	$\log \dot{M}_{\text{mol}}^{\text{a}}$ ( $M_{\odot}$ yr $^{-1}$ )	$\log M_{\text{out}}^{\text{b}}$ ( $M_{\odot}$ )	$\log \dot{M}_{\text{mol}}^{\text{b}}$ ( $M_{\odot}$ yr $^{-1}$ )	$t_{\text{dyn}}$ (yr)	Reference
ISO-Oph 32	SMA	40	$\rho$ Oph	-	-	-	-	-	-	-	1, 2
ISO-Oph 102	SMA	60	$\rho$ Oph	1000	4.7	-4.5	-7.5	-3.3	-6.3	1100	1, 3
2M 0441+2534	CARMA	35	Taurus	-	-	-	-	-	-	-	4, 2
2M 0439+2544	CARMA	50	Taurus	-	-	-	-	-	-	-	4, 2
2M 0438+2611	CARMA	70	Taurus	-	-	-	-	-	-	-	4, 5
GM Tau	SMA	73	Taurus	700	4.6	-5.7	-8.6	-4.5	-7.4	700	6, 5
2M 0414+2811	CARMA	75	Taurus	-	-	-	-	-	-	-	4, 5
MHO 5	SMA	90	Taurus	600	2.1	-4.9	-8.3	-3.7	-7.1	2700	7, 2

REFERENCES. — References for mass estimate, outflow mass and mass-loss rate: (1) Natta et al. (2004); (2) Phan-Bao et al. (2011); (3) Phan-Bao et al. (2008); (4) Muzerolle et al. (2005); (5) this paper; (6) White & Basri (2003); (7) Muzerolle et al. (2003).

NOTE. — <sup>a</sup>Lower limits of outflow mass and mass-loss rate without mass corrections.

<sup>b</sup> Upper limits of outflow mass and mass-loss rate with mass corrections: a factor of three for SMA missing flux (Bourke et al. 2005) and five for optical depth (Levreault 1988a).

TABLE 3  
WIND MASS-LOSS RATE OF YOUNG VLM OBJECTS IN  $\rho$  OPHIUCHI AND TAURUS

Target	$\log \dot{M}_{\text{acc}}$ ( $M_{\odot} \text{ yr}^{-1}$ )	$\log \dot{M}_{\text{wind}}^{\text{a}}$ ( $M_{\odot} \text{ yr}^{-1}$ )	$\log \dot{M}_{\text{wind}}^{\text{b}}$ ( $M_{\odot} \text{ yr}^{-1}$ )	$\dot{M}_{\text{wind}}/\dot{M}_{\text{acc}}^{\text{c}}$	Reference
ISO-Oph 102	−9.0	−8.9	−7.7	1.3-20.0	1
GM Tau	−8.6	−9.9	−8.7	0.05-0.8	2
MHO 5	−10.8	−10.0	−8.8	6.3-100.0	3

REFERENCES. — References for accretion rate: (1) Natta et al. (2004); (2) White & Basri (2003); (3) Muzerolle et al. (2003).

NOTE. — <sup>a</sup>Lower limit of wind mass-loss rate.

<sup>b</sup> Upper limit of wind mass-loss rate.

<sup>c</sup> The range of the ratio of wind mass-loss rate to the accretion rate.